Unified Mathematical Model for Multilayer-Multiframe Compressive Light Field Displays Using LCDs

Jiahui Zhang, Zhencheng Fan, Dawei Sun, and Hongen Liao, *Senior Member, IEEE*

Abstract—We propose a unified mathematical model for multilayer-multiframe compressive light field displays that supports both attenuation-based and polarization-based architectures. We show that the light field decomposition of such a display can be cast as a bound constrained nonlinear matrix optimization problem. Efficient light field decomposition algorithms are developed using the limited-memory BFGS (L-BFGS) method for automultiscopic displays with high resolution and high image fidelity. In addition, this framework is the first to support multilayer polarization-based compressive light field displays with time multiplexing. This new architecture significantly reduces artifacts compared with attenuation-based multilayer-multiframe displays; thus, it can allow the requirements regarding the number of layers or the refresh rate to be relaxed. We verify the proposed methods by constructing two 3-layer prototypes using high-speed LCDs, one based on the attenuation architecture and one based on the polarization architecture. Moreover, an efficient CUDA-based program is implemented. Our displays can produce images with higher spatial resolution with thinner form factors compared with traditional automultiscopic displays in both simulations and experiments.

Index Terms—Compressive light field display, multilayer-multiframe LCD display, optimization methods, polarization-based display

1 Introduction

Recently, light field displays have attracted considerable attention because of their ability to produce a wide range of correct views and correct depth cues, which is an attractive capability in the entertainment, exhibition and medicine [1]. Conventional automultiscopic displays can be separated into two main categories: parallax barrier displays [2] and integral image displays [3], [4]. These displays provide both binocular parallax and motion parallax but usually have low spatial resolution and small field of view. Researchers have tried various approaches to address these limitations, such as adopting multiple projectors [5], [6] or rotating or vibrating optical elements [7] to generate high-resolution images. However, these methods usually significantly increase the cost of the hardware and lead to difficulty in maintaining a thin form factor.

Displays using multilayer liquid crystal displays (LCDs) or high-speed LCDs have become popular in the light field display community at present. Rather than accurately recovering every light ray directly, these displays compress enormous amounts of light field information into stacks of discrete 2D images or sequences of images using modern mathematical methods; this approach is called the compressive light field display method. Three primary technologies are used here: attenuation layers, such as modified LCDs [8] or printed transparencies [9]; polarization layers using modified LCDs [10], [11]; and temporal modulators, such as high-speed LCDs [12] or LCoS displays [13]. These systems can display objects beyond their enclosures with high resolution and wide field of view, at the cost of increased computation. Increasing the number of layers or the refresh rate of the displays can enhance the image fidelity and field of view, but these two methods both have limits. Increase the layer number will also increase both hardware and computation complexity, decrease optical efficiency exponentially. Furthermore, for most off-the-shelf LCDs, the refresh rate has an upper limit of 240 Hz. Considering the 60 Hz human flicker fusion threshold, at most four-frame time multiplexing is allowed, which is not enough for high quality light field display.

Inspired by the Tensor Display [12] and Polarization Fields Display [11], we introduce a unified mathematical model for multilayer-multiframe light field displays that supports both attenuation-based and polarization-based architectures, as shown in Fig. 1. We also propose easily implemented, efficient algorithms for light field decomposition. Our polarization-based multilayer-multiframe display model yields a significantly higher Peak Signal-to-Noise Ratio (PSNR) compared with an attenuation-based display model without an increase in the number of layers or the refresh rate.

1.1 Our Contributions

- We propose a unified framework for describing multilayer-multiframe light field displays based on either an attenuation or polarization architecture and cast

- *J. Zhang, Z. Fan, and H. Liao are with the Department of Biomedical Engineering, School of Medicine, Tsinghua University, Beijing 100084, China. E-mail: {jiahui-z15, fanzc13}@mails.tsinghua.edu.cn, liao@tsinghua.edu.cn.*
- *D. Sun is with the Department of Automation, Tsinghua University, Beijing 100084, China. E-mail: sdw14@mails.tsinghua.edu.cn.*

Manuscript received 4 Sept. 2017; revised 11 Feb. 2018; accepted 23 Feb. 2018. Date of publication 28 Feb. 2018; date of current version 29 Jan. 2019. (Corresponding author: Hongen Liao.)
Recommended for acceptance by K. Myszkowski.
For information on obtaining reprints of this article, please send e-mail to: reprints@ieee.org, and reference the Digital Object Identifier below.
Digital Object Identifier no. 10.1109/TVCG.2018.2810279

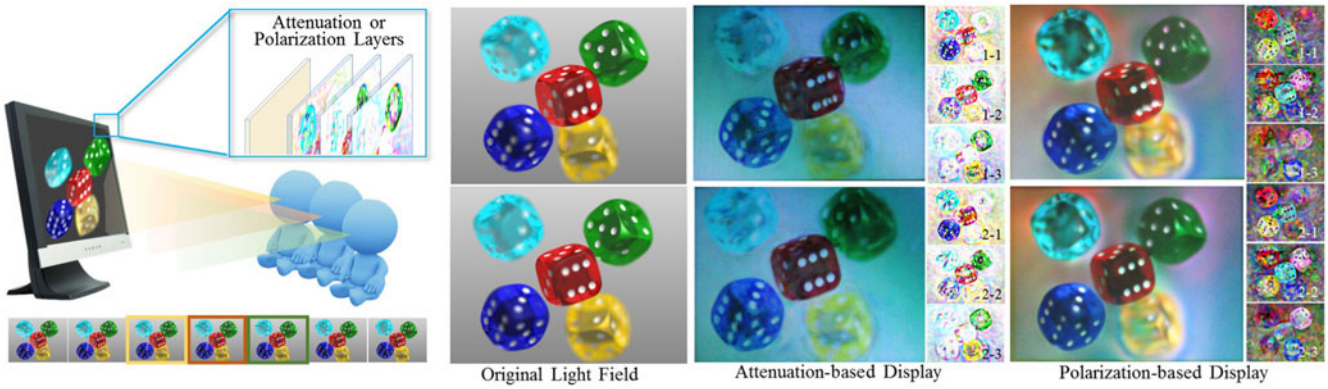

Fig. 1. Automultiscopic display in an attenuation-based or polarization-based multilayer-multiframe architecture. (Left) We introduce a unified mathematical model for multilayer-multiframe light field displays using high-speed LCDs. We develop efficient light field decomposition algorithms and achieve better image fidelity with our polarization-based multilayer-multiframe architecture compared with the traditional attenuation-based architecture. (Right) From left to right: original light field images of different views, photographs of an attenuation-based prototype and the generated layers, and photographs of a polarization-based prototype and the generated layers.

the corresponding problem as a bound constrained optimization problem. We show that the different architectures are represented by different nonlinear forms in the optimization problem.

- We develop efficient light field decomposition algorithms using the L-BFGS method and introduce different methods for handling the bound constraints and initialization in our optimization problem. These methods effectively improve the algorithm performance.
- We construct three-layer attenuation- and polarization-based displays using modified high-speed LCDs and implement an efficient CUDA-based solver.
- Experiments demonstrate that the polarization-based multilayer-multiframe architecture offers significantly increased image fidelity compared with the attenuation-based architecture.

1.2 Overview of Benefits and Limitations

Our unified framework provides new insights into attenuation- and polarization-based multilayer-multiframe displays and enables the derivation of efficient algorithms for light field decomposition. Our displays have multiple benefits, including enhancing the spatial resolution, and maintaining a thin form factor. In addition, we present an efficient solver for light field displays with higher resolution and image fidelity. Our polarization-based display shows better image fidelity without any increase in the hardware cost.

Our displays have the same limitations shared by all multilayer displays, including moiré, color-channel crosstalk, and decreased brightness. Moreover, the polarization-based architecture requires LCDs to behave as polarization rotators; however, the optical characteristics of off-the-shelf LCDs deviate from the ideal model. Additional optical engineering work will be needed for the development of ideal polarization rotators to eliminate artifacts.

2 Related Work

2.1 Attenuation-Based Light Field Displays

Attenuation-based displays use attenuating spatial light modulators to emit light fields. The pinhole arrays or lens arrays used in traditional integral image or parallax barrier displays can be regarded as fixed binary attenuated optical elements. These displays share a limitation of low resolution. In recent years, several researchers have constructed compressive light field displays using stacks of optical attenuation devices, such as attenuating LCD layers [14], [15] or printed transparencies [9], to enhance the resolution of light field displays. Lanman et al. [8] and Wetzstein et al. [12] utilized temporal multiplexing to improve the fidelity of light field displays. They showed that temporal multiplexing can be described via a low-rank matrix or tensor approximation. The tensor representation unifies the multilayer and multiframe architectures; however, it cannot support polarization-based displays. We introduce a unified representation for both attenuation-based and polarization-based architectures, our formulation for attenuation based display describe the same thing with Tensor Display but with a different perspective, one from nonlinear matrix optimization, another from Nonnegative Tensor factorization. And for polarization-based architecture, our experiments show that it can produce higher-quality light field displays.

Meanwhile, there are some reasearches based on attenuation compressive light field display. Chen et al. [16] extended the field of view by means of head tracking. Hirsch et al. [13] presented a compressive light field projector with a passive screen design. Maimone et al. [17] incorporated a high-angular-resolution backlight to provide correct accommodative depth cues. Huang et al. [18] construsted light field stereoscope for virtual reality applications.

2.2 Polarization-Based Displays

Polarization-based displays use the polarization properties of spatial light modulators. Takada et al. [10] constructed a depth-fused 3D display (DFD) using a stack of two twisted nematic (TN) LCDs exploiting the depth-fused 3D phenomenon. Accurate characterization of multilayer LCDs is needed to achieve better DFD performance. Therefore, Date et al. [19] presented a theoretical optical model for the dual-layer LCD structure used in DFDs and measured the luminance addition characteristics of different types of dual-layer LCDs.

Lanman et al. [11] presented the Polarization Field Display design, a light field display that uses a stack of in-plane switching (IPS) LCDs with only the two outermost polarizer films preserved. However, it cannot support

temporal multiplexing. Gotoda [20] improved light field image fidelity without reducing luminance by means of the time-multiplexing translation of a single mirror; their method is equivalent to increasing the number of layers. We use time-multiplexing technology in a manner similar to that of the Tensor Display [12] to improve image fidelity, our work can be seen as extensions of Polarization Field Display to time-multiplexing average cases. These extensions covert original linear optimization problems to nonlinear problems, which are more complicated. We develop corresponding light field decomposition algorithms in accordance with our unified model.

Polarization control devices are also important in many other optics-related areas, such as polarization encoding, optical communication, and biomedical imaging [21]. Moreno et al. [22] constructed a controllable two-dimensional polarization rotator layer using a TN-LCD with additional quarter-wave plates. Aharon and Ofir [21] constructed a wavelength-independent controllable liquid crystal polarization rotator with two nematic LC retarders. These works may provide additional inspiration for improving the performance of polarization-based light field displays.

2.3 Light Field Decomposition Algorithms

Decomposition algorithms are important for computational light field displays and are specific to particular display architectures. The decomposition of a multilayer light field display without time multiplexing can be cast as a linear least-squares problem; therefore, gradient-based algorithms such as the conjugate gradient (CG) method [14] and the trust region method [9] as well as non-gradient-based method such as the Simultaneous Algebraic Reconstruction Technique (SART) [11] can be used. These algorithms are suitable for solving linear equations, however, when going to time-multiplexed displays, the problems are usually nonlinear, which are more complicated. Nonnegative matrix factorization (NMF) [8] and nonnegative tensor factorization (NTF) [12] are applied for light field decomposition. A fast NTF method that uses the proximal gradient method and low-rank approximation has been proposed by Zhou et al. [23]. The authors of [24] evaluated three methods of weighted NMF and concluded that the weighted rank-1 residue iterations (WRRI) method outperformed the other two. But for our polarization-based multiframe display, NTF related methods can not be applied. In this paper, we treat both multiframe attenuation-based and polarization-based architecture as nonlinear non-convex problems with bound constraint. Through attenuation-based architecture has been well illustrated, we revisit this problem from nonlinear optimization perspective and give close result. This process gives us inspiration to deal with multiframe polarization-based architecture.

Usually, computational displays require huge computational resources, Heide et al. [25] proposed a universal adaptive image synthesis framework to lower computational resources for these displays. Through iterative sampling, optimization and adaptation, only few light rays are computed each time. This framework can be used not only for light field displays but also for high dynamic range displays, among others, and it could also be applied to our displays.

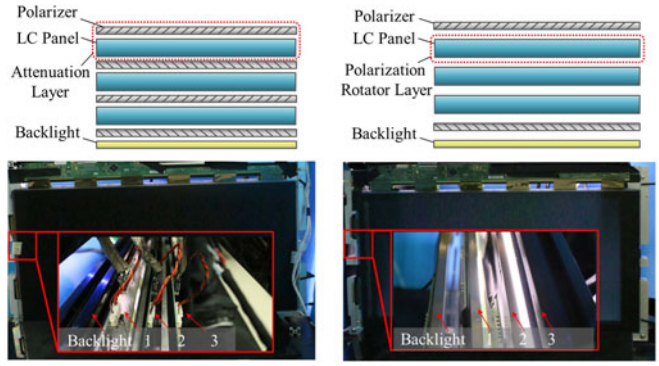

Fig. 2. Attenuation-based and polarization-based displays using LCDs. (Top, left) An attenuation-based display has a uniform backlight and several attenuating layers consisting of LC panels and polarizers. Adjacent polarizer films are crossed. (Top, right) A polarization-based display has a multilayer LC panel serving as polarization rotator layers. Two crossed polarizers are needed at the front and rear of the display. (Bottom, left) An attenuation-based prototype constructed by removing the polarizers from the second LCD. (Bottom, right) Polarization-based prototype constructed by removing all polarizers except the two outermost ones.

3 Multilayer-Multiframe Light Field Displays

This section presents a unified framework for multilayer-multiframe light field displays that uses a nonlinear optimization model. We also derive corresponding light field decomposition algorithms for these displays. First, we present an introduction to multilayer-multiframe light field displays based on either an attenuation or polarization architecture using LCDs and describe how these architectures emit 4D light fields. Second, we introduce how to represent these architectures with a unified bound constrained nonlinear optimization model. Third, optimization algorithms corresponding to these two architectures are clarified. Finally, initialization methods to improve the efficiency of the optimization algorithms are discussed.

3.1 Multilayer-Multiframe Light Field Displays Using LCDs

An LCD consists of a uniform backlight and an LC panel sandwiched between two orthogonal linear polarizer films. The LC panel can change the polarization states of light rays and can be roughly regarded as a programmable polarization rotator layer. An attenuating layer is formed by combining an LCD panel with a polarizer film. A multilayer display is an extension of a single-layer display that usually consists of one uniform backlight and multiple layers of LC panels and polarizer films. Fig. 2 shows the architectures of our displays, which are similar to those of [11] except that our architectures support time multiplexing. An attenuation-based display consists of multiple attenuating layers; the polarizer films of adjacent layers are usually crossed so that each layer can be operated in the same manner as a common single-layer LCD. A polarization-based display has multiple polarization rotator layers and only two crossed polarizer films enclosing these LC panels. The different architectures rely on different modes of light modulation. Here, we first introduce how an attenuation-based multilayer-multiframe display emits a 4D light field.

A light field is usually described as a 4D function; we adopt the definition $L(v_x, v_y, r_i, r_j)$ for simplicity, where v_x

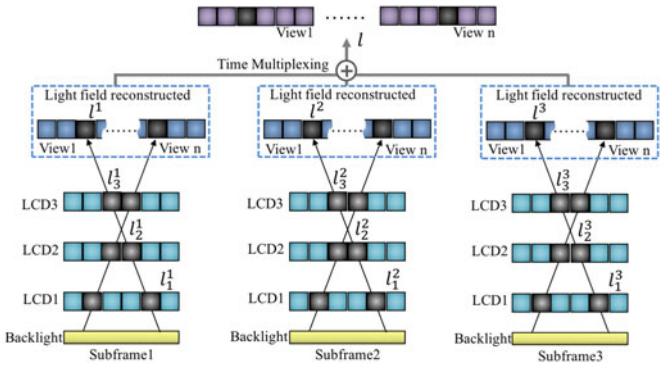

Fig. 3. Light path in a three-layer, three-frame attenuation-based display. The perceived luminance of light ray l is given by Eq.1. The light is attenuated after passing through each layer, and the viewer perceives the time average of each frame. The operation of a polarization-based display is based on a similar principle but with a different mode of light modulation.

and v_y represent the horizontal and vertical view angles, respectively. For a specific view, $L(r_i, r_j)$ represents the oblique projection image captured in this view. The multilayer LCDs approximate the target light field by modulating the uniform light rays produced by the backlight. When high-speed LCDs rapidly display multiple images, a viewer will perceive the time average of those images [12]. Thus, for an M-layer, N-frame attenuation-based light field display as shown in Fig. 3, the perceived luminance of pixel (r_i, r_j) in view (v_x, v_y) can be described as follows:

$$l = L(v_x, v_y, r_i, r_j) = \frac{1}{N}\sum_{n=1}^{N}\prod_{m=1}^{M} l_m^n, \tag{1}$$

Each pixel need to generate several light rays in different directions, $l_m^n \in [0, 1]$ is the transmittance of the pixel where light rays intersect with layer m in frame n. Because the required transmittances for each light may be different and confilct with each other, we need to minimize these conflicts overall. Increasing the number of layers or the number of frames can improve the image quality of the recovered light field because of the increased degrees of freedom.

3.2 Representation of an Attenuation-Based Light Field Display

Although the operation of multilayer-multiframe attenuation-based light field displays is already well illustrated by the Tensor Display [12], we introduce a new formulation for this architecture from another perspective and present an efficient corresponding solver. Importantly, the proposed formulation and solver can be easily extended to describe multilayer-multiframe polarization-based displays, which have not been studied previously.

Our representation is inspired by [9], [14]. We rewrite Eq. (1) as follows:

$$l = \frac{1}{N}\sum_{n=1}^{N} exp\left(\sum_{m=1}^{M}\xi_m^n\right), \tag{2}$$

where

$$\xi_m^n = \log l_m^n \in (-\infty, 0], \tag{3}$$

represents absorbance as described in [9]. Eq. (2) represents the formation of a single light ray. To describe the entire light field, we can expand Eq. (2) in matrix form as follows:

$$\widetilde{L} = \frac{1}{N}\sum_{n} f(Ax_n) = \frac{1}{N} f(Ax)E. \tag{4}$$

Here, the following notation is used:

- $\widetilde{L}$ is the recovered light field.
- x is a matrix in which each element $x_{mn} = \xi_m^n$ represents the transmittance of an LCD pixel in logarithmic space.
- x_n is the Nth column of x and contains the pixels in all layers of one frame.
- A is a sparse projection matrix, where

$$A_{ij} = \begin{cases} 1 & \text{if light ray i passes through pixel j,} \\ 0 & \text{otherwise.} \end{cases} \tag{5}$$

- $f(x)$ is an element-wise operation function. For an attenuation-based display, $f(x)$ can be described as follows:

$$f(x) = exp(x). \tag{6}$$

- $E_{N\times 1}$ is an all-one vector; consequently, this matrix multiplication operation sums all columns.

As indicated previously, we minimize the overall error to approximate the original light field:

$$x = arg\ \min_x \frac{1}{2}\|f(Ax)E - Nb\|^2, x \le 0, \tag{7}$$

where b represents the target light field image pixels stacked in one column. The solution to this bound constrained optimization problem provides an optimal layer images in the least-squares sense. Note that this is a bound constrained optimization problem, the arguments must be non-positive.

3.3 Optimization Algorithm

In previous works, SART, trust region method were used for light field display. But because our problems are nonlinear problems, SART method is not suitlable. Trust region method needs to compute Hessian matrix, which is very complicated and time-consuming in our nonlinear large scale case. So, we need to find new method for our problems. Many algorithms have been proposed for solving large-scale unconstrained nonlinear optimization problems, such as the quasi-Newton method and the conjugate gradient method. Here, we adopt the L-BFGS algorithm, a quasi-Newton method that is popular in areas of machine learning such as log-linear modeling [26]. Unlike in the Newton method, in the L-BFGS method, the Hessian matrix is approximated using gradient information collected from a limited number of previous iterations, and then a linear search is conducted to minimize the cost function. Besides, we also test CG method, and it get close results with L-BFGS, see Appendix A, which can be found on the Computer Society Digital Library at http://doi.ieeecomputersociety.org/10.1109/TVCG.2018.2810279 for details.

Regarding the light field decomposition problem, in previous works [11], [12], the variables have simply been projected into the feasible region after each iteration. However, we find that this method may result in slow convergence or even failure in our case, as Fig. 4 shows. It usually falls into local minimum as observed in our experiments, the solver

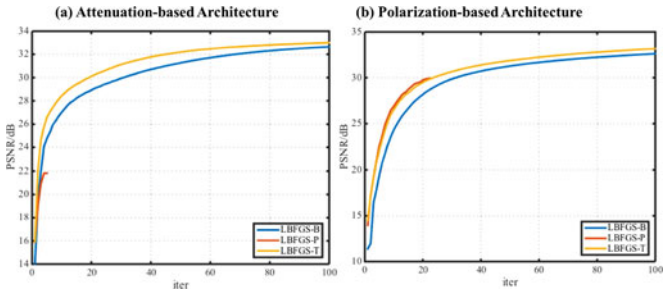

Fig. 4. Performances of different methods of handling the bound constraints of our optimization problems: projecting variables into a feasible region after each iteration (L-BFGS-P), the L-BFGS-B method, and the L-BFGS method with variable transformation (L-BFGS-T). (a) Experiment using an attenuation-based display. (b) Experiment using a polarization-based display.

which is intended for non-constrained optimization might search a wrong direction and step size for our bound constrained problem. Another straightforward idea for solving this constrained optimization problem is to apply the L-BFGS-B algorithm, which is an extension of the L-BFGS method to handle bound constraints [27]. It uses the gradient projection method to determine a set of active variables, which will be held at the bounds, and minimizes the error at the free variables. Here, we test a simple method of handling bound constraints and find that it is effective and efficient. We adopt the following variable transformation:

$$x = -y^2. \tag{8}$$

This converts the problem into an unconstrained problem. Then, we apply the L-BFGS method. This method results in faster convergence than the L-BFGS-B method, as shown in Fig. 4. Variable transformation is a common technique and can be a useful method for constrained problems in which the constraints have simple forms [28].

We wish to minimize the following cost function using the L-BFGS method:

$$h(x) = \frac{1}{2}\|f(Ax)E - Nb\|^2. \tag{9}$$

To do so, we need to provide gradient information $\frac{\partial h}{\partial x}$. The derivative of $h(x)$ with respect to x_{ij} is

$$\frac{\partial h}{\partial x_{ij}} = r^T \begin{bmatrix} A_{1i} f'(z_{1j}) \\ \vdots \\ A_{Pi} f'(z_{Pj}) \end{bmatrix}, \tag{10}$$

where

$$r = f(Ax)E - Nb, z = Ax. \tag{11}$$

Written in matrix form, the entire gradient can be expressed as follows:

$$\frac{\partial h}{\partial x} = A^T diag(r) f'(z), \tag{12}$$

where $diag(r)$ is a diagonal matrix with the elements of vector r on the main diagonal.

Considering the variable transformation given in Eq. (8) and substituting Eq. (6) into Eq. (12), we obtain the final equation:

$$\frac{\partial h}{\partial y} = \left[A^T diag(r) exp(z)\right] \circledast (-2y), \tag{13}$$

where $\circledast$ is the Hadamard product. We feed this gradient into the L-BFGS solver.

We have also tested transformations such as $x = -|y|$, but they do not perform well, perhaps because of gradient discontinuity.

3.4 Expanding Our Framework to Polarization-Based Displays

Various methods of 3D image synthesis for polarization-based multilayer displays have been considered [10], [11]. Inspired by the Polarization Field Display technique [11], we expand our framework to a multilayer-multiframe polarization-based architecture. In this new architecture, a time-multiplexing technique is introduced to eliminate artifacts using high-speed LCDs.

As Fig. 2 shows, the polarization-based display lacks the inner polarizer films included in the attenuation-based display. This difference not only improves light transmittance but also introduces a completely new mode of light modulation. In the ideal optical model, each LCD layer is regarded as a polarization rotator layer, which applies a rotation to an incident polarization state. For a single-layer LCD, the intensity of the light after it passes through the second polarizer obeys Malus' law:

$$I = I_0 \sin^2(\theta), \tag{14}$$

where I_0 is the luminance of the uniform backlight, which can be taken to be 1, and θ is the rotation angle applied by the liquid crystal, which is limited to a range of $[0, \frac{\pi}{2}]$ due to the limitations of most commercial LCDs [11]. The multilayer-multiframe polarization-based light field display architecture works much like the attenuation-based architecture except for the light modulation mode. Similarly, we can use a bound constrained nonlinear optimization model to describe our new multilayer multiframe polarization-based architecture:

$$x = arg\ \min_x \frac{1}{2}\|f(Ax)E - Nb)\|^2, 0 \le x \le \frac{\pi}{2}. \tag{15}$$

Here, the following notation is used:

- x represents the polarization rotation angles of all pixels.
- $f(x)$ is again an element-wise operation function, now representing the polarization rotator architecture:

$$f(x) = \sin^2(x). \tag{16}$$

Thus, the corresponding gradient information for the cost function is given by

$$\frac{\partial h}{\partial x} = A^T diag(r) \sin(2z), \tag{17}$$

where r and z are as given in Eq. (11).

Similarly, the following variable transformation is applied to achieve better convergence performance:

$$x = \frac{\pi}{2} \sin^2(y). \tag{18}$$

As Fig. 4 shows, according to our tests, the projection method (L-BFGS-P) can easily become stuck in a local minimum, whereas the L-BFGS-B method yields a similar result but is slower than the L-BFGS method in each iteration. We have also tested transformations such as $x = \arctan y^2$ and $x = \frac{\pi}{4}(\sin y + 1)$, but Eq. (18) performs best.

Thus far, we have presented a unified framework for multilayer-multiframe light field displays that includes both attenuation-based (Eq. (7)) and polarization-based (Eq. (15)) architectures. The different architectures correspond to different nonlinear forms in the nonlinear optimization problem.

3.5 Initialization of the Optimization Algorithm

Initialization plays an important role in optimization; especially in nonlinear, nonconvex optimization, good initialization can lead to faster convergence and even better results. Here, we introduce two initialization methods to improve our optimization algorithm performance.

A straightforward method of initialization is to use random variables drawn from a uniform distribution, as done in [8]. However, this method does not consider any information about the display architecture.

Here, we assume that the pixels of the target light field follow a uniform random distribution and that the energy is equally split among each layer and each frame. More specifically, the target light field pixels follow

$$l \sim U(0, 1). \tag{19}$$

For an attenuation-based display, all pixels in each layer and each frame matter equally. Thus, from Eqs. (2) and (3), we can derive that the argument of the objective function expressed in Eq. (7) should follow

$$\xi = \log\left(l^{\frac{1}{M}}\right), \tag{20}$$

where l obeys Eq. (19). Therefore, we can initialize the arguments by applying a transformation as shown in Eq. (20) to a set of uniform random variables. The experimental results presented in Fig. 5 demonstrate the effectiveness of the proposed method.

Similarly, for a polarization-based display, we have

$$l = \frac{1}{N}\sum_{n=1}^{N} \sin^2\left(\sum_{m=1}^{M} \theta_m^n\right), \tag{21}$$

where l again follows the distribution in Eq. (19) and all θ_m^n matter equally.

Because the function $\sin^2(\theta)$ is periodic (with a period of π) on $\left[0, \frac{M\pi}{2}\right]$, to simplify the initialization, we ignore the summation of the rotation angles, yielding the following distribution of rotation angles:

$$\theta = \arcsin\left(\sqrt{l}\right) \in \left[0, \frac{\pi}{2}\right]. \tag{22}$$

Although this simplification is not rigorous, the experimental results presented in Fig. 5 demonstrate the effectiveness of the proposed initialization method, which can result in a higher PSNR.

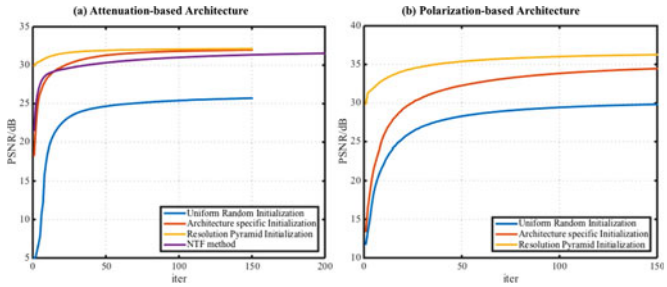

Fig. 5. Performances of different initialization methods: initialization with random uniform variables, initialization using Eq. (20) or Eq. (22), and initialization using the pyramid method. (a) Experiment using an attenuation-based display; the results of the NTF method are also shown. (b) Experiment using a polarization-based display.

Moreover, there are several commonly used initialization methods in the image processing domain. The image pyramid method is a multiscale analysis method used in many areas [29], [30], [31], which can produce robust results for large-scale problems and accelerate calculations to some extent. We adopt an approach similar to that used in [32] for the decomposition of a multilayer light field display. The original light field forms the lowest level of the pyramid. Higher levels of the pyramid are constructed by downsampling from the spatial resolution of the previous level while leaving the angular resolution unchanged. Here, we employ the simplest bilinear interpolation method as the sampling method. During sampling, we also ensure that the physical size of the light field and the display gap remain unchanged. Optimization at lower resolution is easier because of the reduction in the parameter dimensionality. The highest level of the pyramid is initialized using the previously proposed method, and the result for each level of the pyramid provides a coarse initialization for the next lower level. The performance of the image pyramid method is shown in Fig. 5; For attenuation display, pyramid initialization can only speed up optimization, but for polarization display, pyramid initialization can also give higher PSNR, which means polarization architecture is more sensitive to initialization. More detailed results on the effects of initialization can be found in Section 5.1.

4 Implementation and Assessment

This section describes our hardware and software implementations of multilayer-multiframe light field displays based on our attenuation and polarization architectures. We also present detailed results of simulations and prototype experiments.

4.1 Hardware

We built our prototypes using modified Acer XB240H 144 Hz TN-LCD panels with a resolution of 1920×1080 (see Fig. 2). The uniform backlights were obtained from the disassembled monitors. Both polarizer films were removed from the middle LC panel to ensure that adjacent polarizers were crossed in the attenuation display. All of the polarizer films except the two outermost ones were removed to construct the polarization display. Aluminum frames were milled and used to mount the LC panels. The spacing between layers was fixed at 1.5 cm using acrylic spacers, yielding a thin form factor with a total thickness of 3 cm. We gave a rough calibration

using the moiré fringe calibration method proposed by Hirsch et al. [33]. Gamma value was also calibrated, but black level was not calibrated and considered in our update rules, which may slightly influence the quality.

We implemented a MATLAB-based offline algorithm and an online algorithm using CUDA. The results presented below were all obtained on an Intel Core i7 workstation with 32 GB of RAM and a GTX Titan X graphics card.

4.2 Software

The target light fields were obtained from the Synthetic Light Field Archive[1] with a spatial resolution of 512×384 pixels and an angular resolution of 7×7 views. All images were rendered via oblique projection within a field of view of 10 degrees.

For our offline MATLAB algorithms, L-BFGS and L-BFGS-B, described in Section 3.3, we used the implementations given in [34], [35]. We used a pyramid with five levels of resolution to initialize the optimization and performed 10 iterations on the four highest levels of the pyramid for initialization. A MATLAB NTF algorithm was also implemented for comparison using the Tensor Toolbox [36]. The multiplicative update rules used by Wetzstein et al. [12] were adopted, and the values were clamped to the feasible region after each iteration. The RGB channels were handled sequentially.

In addition, a rough-online GPU implementation using CUDA-L-BFGS [37] for computation and OpenGL for rendering was also created for further acceleration.

4.3 Results

It takes approximately 2.5 minutes to decompose a color light field into three-layer, three-frame sequences with 50 iterations using MATLAB, and another 8s to initialize using pyramid method, each iteration takes about 1s. The GPU implementation can achieve an acceleration of approximately 70 times compared with the offline MATLAB implementation for three-frame decomposition, up to 7 HZ with 10 updates. Most time (more than 80 percent are spent on gradient computation). Simulated results for attenuation- and polarization-based displays are shown in Figs. 6 and 7, respectively. Motion parallax can be observed, as shown in Fig. 1; no flicker is observed when using three-frame time multiplexing with our 144 Hz LCDs. Smooth motion parallax can be seen in the supplementary video (prototype.mp4), available online.

We conducted quantitative experiments on six different scenes, with the results shown in Table 1. For attenuation-based display, our method yields slightly higher PSNRs than the NTF method. Fig. 5 also shows the convergence performance of our method and the NTF method. For polarization-based display, the experimental results show that the image quality can be significantly improved with time multiplexing and that the PSNRs are higher than those achieved via attenuation-based display. Specifically, the average PSNRs for polarization display are higher than those for attenuation display by 3.79, 5.41, 7.92, and 11.22 dB for 2-, 3-, 6-, and 12-frame time multiplexing,

1. http://web.media.mit.edu/~gordonw/SyntheticLightFields/

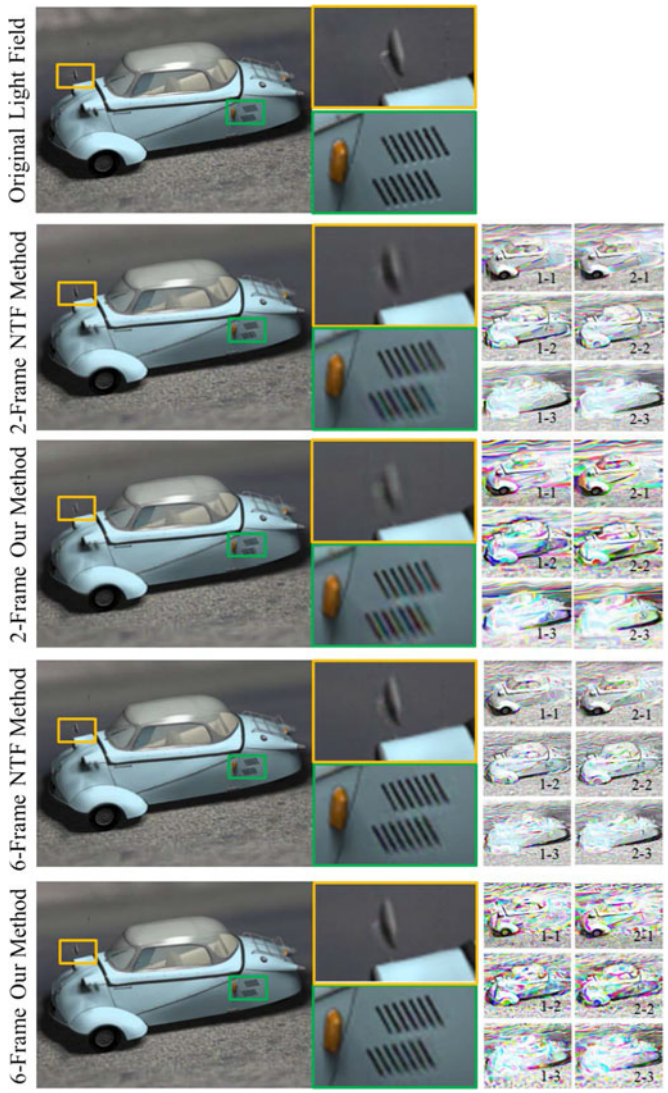

Fig. 6. Decomposition results of the NTF method and our method for a three-layer attenuation-based display. From left to right: original and recovered central views of the "messerschmitt" scene, details of the recovered light field image, and the temporal frames of the three layers. Similar recovered light fields are obtained using our method and the NTF method.

respectively. We find that even a two-frame polarization display can achieve better image fidelity than a 12-frame attenuation display on average, meaning that the same display effect can be achieved with a lower refresh rate or fewer layers. This is meaningful considering the upper limit on the LCD refresh rate. Besides, we have also conducted stability experiments, and find that our method converge stably. The fluctuation of results is within ± 0.03 dB for attenuation-based architecture, and ± 0.42 dB for polarization-based architecture. Though the stability of results for polarization-based architecture is a little worse than attenuation-based display, polarization-based display can give significantly higher PSNR.

However, artifacts were observed in the prototype experiments, see Fig. 9. On the one hand, this may be because of our imprecise display calibration and color distortion when photographing, on the other hand, we attribute these artifacts to the deviation of the actual multilayer TN-LCDs from the ideal polarization rotator model, which will be discussed in Section 5.3.

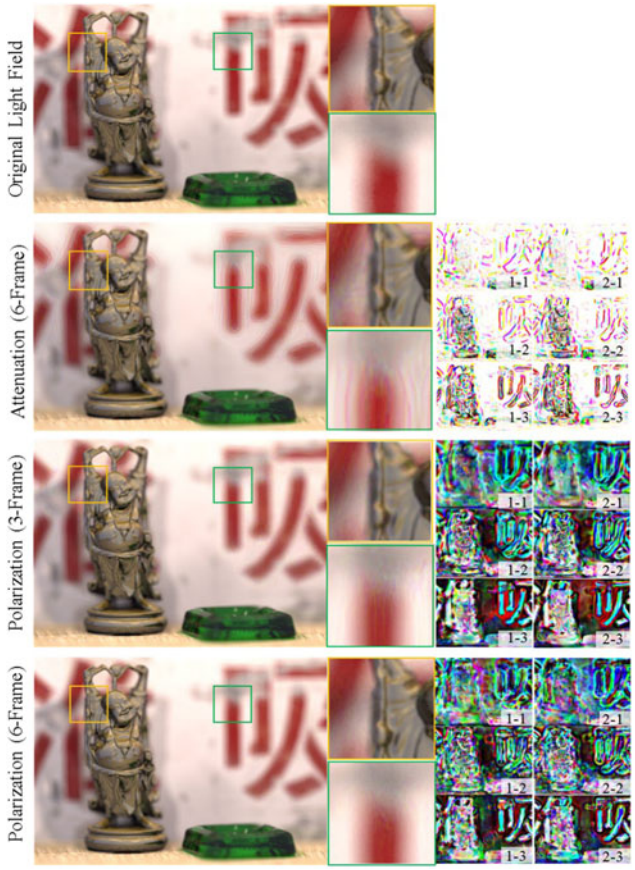

Fig. 7. Decomposition results for three-layer, multiframe displays. From top to bottom: central view of the "happy buddha" scene, decomposition results for a six-frame attenuation-based display, and decomposition results for three-frame and six-frame polarization-based displays. The details of the recovered images and displayed layers are presented. Halo artifacts are reduced in the polarization-based displays.

4.4 Comparison with Other Methods

This section gives more detailed results about the comprasion of the proposed L-BFGS based method with other methods.

Fisrt is SART method, as we have explained above, it can only be applied to linear problems and is not suitable for our problems. However, because our methods can also be used for linear problems, here we also give a comparison with SART in linear case, see details in Table 2. As the table shows, our method gives higher PSNR in attenuation-based display, but gets a little worse results than SART in polarization case. But when goes to multi-frame case, our method can easily give higher PSNR as Table 2 shows.

TABLE 2
Comparison with SART Method

	Method	Dice	Dragon	Happy Buddha
Attenuation 1-Frame	SART	28.10	22.93	25.73
	L-BFGS	29.54	24.61	26.47
Attenuation 3-Frame	SART	N	N	N
	L-BFGS	32.13	26.39	27.66
Polarization 1-Frame	SART	29.60	25.56	27.99
	L-BFGS	28.46	25.92	26.58
Polarization 3-Frame	SART	N	N	N
	L-BFGS	36.26	33.98	34.89

Both PSNR(/dB) for one-frame display and three-frame display are given, "N" means SART method can not be used for nonlinear problem.

Besides, We have also test conjugate gradient method. In our experiments, it performance similarly as L-BFGS method, which means, it will also convergences slowly or even fails when directly project variables to feasible region after each iteration, and initialization also effects the optimization results especially in polarization case. When we apply the techniques (initialization method and bound constraint handling method) used in the paper, CG method gets almost the same results with L-BFGS in average (we repeat this for five times), this experiment once again shows the effectiveness of the proposed skills, see Table 3 for detailed results.

5 Discussion and Future Work

This section presents more detailed investigations of the differences between our solver and the previously developed NTF method and the differences between attenuation- and polarization-based displays. We also discuss the benefits

TABLE 1
Quantitative PSNR (dB) Results for Different Methods of Light Field Recovery: The NTF Method for Attenuation-Based Display (NTF), Our Method for Attenuation-Based Display (Attenuation), and Our Method for Polarization-Based Display (Polarization)

	Data	butterfly	dice	dragon	happy buddha	messerschmitt	xyzrgb dragon	average
2-Frame	NTF	31.02	31.55	25.61	24.82	30.56	25.79	28.22
	Attenuation	31.36	31.87	25.69	24.94	30.88	25.89	28.44
	Polarization	33.90	34.08	31.45	29.99	32.47	31.51	32.23
3-Frame	NTF	32.12	32.44	26.38	25.50	31.60	26.18	29.04
	Attenuation	32.58	32.87	26.50	25.61	31.97	26.26	29.30
	Polarization	37.02	36.06	33.96	32.32	34.68	33.67	34.71
6-Frame	NTF	33.62	33.76	28.00	26.63	32.92	26.72	30.28
	Attenuation	34.43	34.34	28.36	26.89	33.59	26.88	30.75
	Polarization	41.16	40.66	37.28	36.79	38.87	37.27	38.67
12-Frame	NTF	34.82	34.84	29.04	27.38	34.14	27.43	31.28
	Attenuation	35.81	35.55	29.40	27.74	34.85	27.67	31.84
	Polarization	47.51	45.29	39.97	41.85	44.39	39.37	43.06

Different numbers of frames for time multiplexing were tested. The numbers of iterations for 2, 3, 6, and 12 frames are respectively 200, 300, 400, and 600 for the NTF method and 100, 150, 300, and 500 for the proposed L-BFGS-based method for both the attenuation and polarization displays. The PSNR was computed by considering all RGB channels together. Even a two-frame polarization display can achieve better image fidelity than a 12-frame attenuation display on average, as shown in red.

TABLE 3
CG Method Performance

Data		Dice	Dragon	Happy Buddha
Attenuation/ dB	Random Initiation	31.35	25.82	26.93
	Projection	19.81	17.05	17.54
	CG	32.14	26.40	27.67
	L-BFGS	32.13	26.39	27.66
Polarization/ dB	Random Initiation	30.46	28.95	31.59
	Projection	31.14	28.57	29.25
	CG	36.26	33.98	34.88
	L-BFGS	36.26	33.98	34.89

"Random Initialization" represents start CG method with random initialization; "Projection" represents project variables to feasible region after each iteration with CG method; "CG" represents using CG method with the proposed skills in our paper; "L-BFGS" is a baseline for comparison using method described in the text.

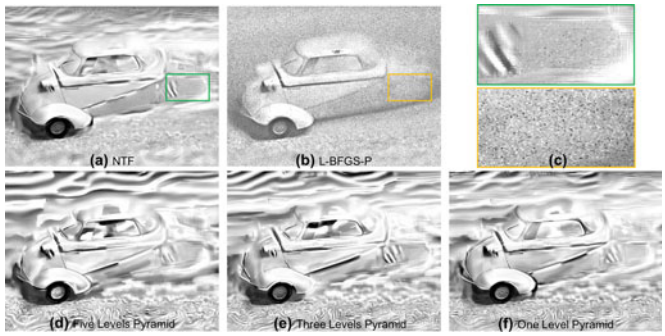

Fig. 8. Decomposition results for different methods of attenuation display. (a) NTF method. (b) L-BFGS with projection of variables to the feasible region (L-BFGS-P). (c) Details of the selected regions in (a) and (b). (d)-(f) L-BFGS with pyramid initialization using pyramids with different numbers of levels.

and limitations of our work. Future work on both the algorithms and hardware will be needed to improve display performance.

5.1 Differences between Our Solver and the NTF Method

Fig. 8 shows the light field decomposition results for different optimization methods for attenuation-based displays. Although nearly identical PSNRs are achieved, we can observe different characteristics in the decomposition results; see Figs. 8a and 8d. Speckles are clearly visible in the NTF results, whereas there are no obvious speckles in our results. Moreover, the fringes in our results seem markedly wider than those in the NTF results.

We attribute the appearance of speckles to the clamping of values to the feasible region after each iteration, as this can cause pixel discontinuity. In our method, the speckles disappear because the proposed variable transformation method avoids bound constraints. If we apply the projection method in combination with L-BFGS, speckles will again be present; see the results for the L-BFGS-P method in Fig. 8b. This observation confirms our explanation for the appearance of speckles.

We believe that the wider fringes are mainly caused by the resolution-pyramid-based initialization method. Details are lost in the higher levels of the pyramid because of downsampling, and this effect will be passed on to the lower levels of the pyramid; thus, the fringes become larger as details in the corresponding regions are lost. Figs. 8d, 8e, and 8f show the results of applying the resolution-pyramid-based initialization method with different numbers of levels in the pyramid. The fringes become smaller as the number of levels decreases, confirming our interpretation. A more refined sampling method, such as a Gaussian pyramid method or a Laplacian pyramid method, might provide more accurate initialization for high-resolution analysis and thus yield better results, as these methods can retain more information when the resolution is reduced. Differences other than speckles still exist between Figs. 8a and 8f; this may be because the two solvers converge to different minima.

5.2 Differences between Attenuation-Based and Polarization-Based Displays

The experimental results in Table 1 show that a polarization-based display can produce a higher PSNR than an attenuation-based display. More specifically, we find that the polarization-based approach can eliminate halo artifacts around high-contrast edges, which are observed only in the recovered light field images from the attenuation-based architecture; see Fig. 7. This phenomenon has also been reported in multilayer polarization displays without time multiplexing [11]. Lanman et al. proposed that these halo artifacts may be caused by nonlinear form introduced by logarithmic transformation in the cost function, which will penalize artifacts in regions with small image values. In addition, we believe that another reason for the higher PSNRs of the polarization-based architecture may be its greater flexibility, as in the polarization rotator model, each pixel can not only attenuate luminance but can also enhance luminance after passing a new layer, but for attenuation-based display, it can only attenuate luminance after passing one layer. In high-contrast edegs, black region and bright region both exist. For attenuation-based display, the bright region requires all these layers to have a high transmission, but the black region requires these layers to have a low transmission, attenuation architecture may can't handle this case properly. But for polarization-based display, as it is more flexible, it may find a balance to distribute the polarization angle of each layer. Further analysis in the frequency domain, as done in [12], may help to elucidate the origin of the PSNR improvement. Following Polarization Field Display [11], we hope to attract more attention on polarization based architecture because of the better flexibility it provide and the potential of giving high quailty display.

Finally, although the multilayer-multiframe polarization architectures have already enabled remarkable PSNR enhancements, there is still space for further improvement. As the experiment presented in Fig. 5b shows, our algorithm may easily become trapped into different local minima depending on initialization. A better optimization strategy may help to avoid these local minima, resulting in higher PSNRs.

5.3 Deviations of the Prototype from the Ideal Polarization Rotator Model

Current consumer LCDs are available in different types, such as TN panels, IPS panels, and patterned vertical alignment panels. Traditionally, LC panel is seen as polarization rotator layer, which can induce a rotation of the polarization

Fig. 9. Photographs of our three-layer, three-frame display prototypes. (Top) Attenuation-based display. (Bottom) Polarization-based display. Artifacts are evident in the polarization-based display.

angle of light rays traversing the pixel [11]. However, the behavior of single LC panel and multilayer LC panel are actually more complicated. For example, single domain LCD is characterized as rotated half-wave plate [11], [19]. For TN panels used in our work, Date et al. [19] measured the luminance addition characteristics of dual-layer LCDs and roughly described this architecture as polarization rotator model. Lanman et al. [11] presented a theoretical analysis of multilayer TN-LCDs in the supplementary material, available online, and concluded it as counterbalanced rotation layer model. Moreno et al. [22] constructed a controllable two-dimensional polarization rotator layer using a TN-LCD with additional quarter-wave plates, but it seems they use a different optical model with previous two works.

We adopt the polarization rotator model presented by Date because it is more consistent with the results observed in our experiments and gives acceptable results. However, artifacts still exist, as Fig. 9 shows. We observed that such artifacts mainly occur in regions where two or three layers have large rotation angles (bright regions). As mentioned above, our solver is easily influenced by initialization; therefore, we applied a temporary method to eliminate artifacts. We limited the rotation angles by specifying small initial values, thus ensuring that the decomposition layers would have smaller values. As a result, the artifacts were reduced to some extent, as shown in Fig. 10. Furthermore, because TN-LCDs have poor viewing angle characteristics, vertical parallax was not properly achieved in our prototype experiments.

We think at least, there is no agreed standard answer for the optical model of multilayer polarization-based displays among these published works. Also, for the IPS-LCDs used in Polarization Field Display [11], both polarization rotators model and multi-domain model are tried, but both prototypes have color artifacts. Thus, the question of which type of LCD is best for polarization-based multilayer displays also needs to be further explored. Theoretical obstacle might not exist, but much more effort is needed to give convinced results both in theory and practice for these problems. In addition, as mentioned in Section 2.2, research in other areas may help to achieve the construction of ideal multilayer polarization-based displays.

Fig. 10. Photographs of prototypes after correction by means of limiting the layer rotation angles. Artifact reduction can be observed in comparison with Fig. 9.

5.4 Future Work

As discussed above, there are still further questions worthy of exploration. A more efficient optimization algorithm is needed for higher-resolution display, and there is still room to enhance the PSNR of the polarization-based architecture. Using the sampling strategy proposed by Heide et al. [25] may help to achieve a real time update for practical display. Beside, according to [12], [38], analysis in the frequency domain may be helpful for theoretically estimating the field of view and various limitations of our displays.

In terms of hardware, additional optical instrumentation can be applied to enhance display performance, such as directional backlighting [12]. In addition, constructing multilayer polarization rotators that are closer to ideal using additional optical elements may be a promising way to eliminate artifacts. Furthermore, if each pixel could apply a full range of rotation, namely, $[0, \pi]$, bound constraints would be eliminated from the optimization problem, which might significantly improve display performance. One simple idea is to combine two LCDs into a single display.

6 Conclusion

In conclusion, we have presented a unified framework for multilayer-multiframe light field displays that supports both attenuation-based and polarization-based architectures. In addition, we provided efficient light field decomposition algorithms. We demonstrated the potential of polarization-based multilayer displays with temporal multiplexing, which can allow higher image fidelity to be achieved without increasing the number of layers or the refresh rate. The realization of multiple ideal full-range polarization rotator layers will enable the elimination of artifacts and the construction of better automultiscopic displays.

Acknowledgments

This work was supported in part by National Key Research and Development Program of China (2017YFC0108000), National Natural Science Foundation of China (81427803, 81771940), Beijing Municipal Science & Technology Commission (Z151100003915079), Beijing Municipal Natural Science Foundation (7172122), and Soochow-Tsinghua Innovation Project (2016SZ0206). We thank the reviewers for their suggestion. Helpful advice was provided by Guowen Chen, Xinran Zhang, Tianqi Huang, and Cong Ma with Department of Biomedical Engineering, School of Medicine, Tsinghua University.

REFERENCES

[1] H. Liao, T. Inomata, I. Sakuma, and T. Dohi, "3-D augmented reality for MRI-guided surgery using integral videography autostereoscopic image overlay," *IEEE Trans. Biomed. Eng.*, vol. 57, no. 6, pp. 1476–1486, Jun. 2010.

[2] F. E. Ives, "Parallax stereogram and process of making same," 1903.

[3] G. Lippmann, "Epreuves Reversibles Donnant la Sensation du Relief," *J. De Physique Théorique Et Appliquée*, vol. 7, no. 1, pp. 821–825, 1908.

[4] H. Liao, T. Dohi, and K. Nomura, "Autostereoscopic 3D display with long visualization depth using referential viewing area-based integral photography," *IEEE Trans. Vis. Comput. Graph.*, vol. 17, no. 11, pp. 1690–1701, Nov. 2011.

[5] H. Liao, M. Iwahara, N. Hat, I. Sakuma, T. Dohi, T. Koike, Y. Momoi, T. Minakawa, M. Yamasaki, and F. Tajima, "High-resolution integral videography autostereoscopic display using multi-projector," in *Proc. 9th Int. Display Workshop*, vol. 136, no. 5, 2002, pp. A–194.

[6] K. Nagano, A. Jones, J. Liu, J. Busch, X. Yu, M. Bolas, and P. Debevec, "An autostereoscopic projector array optimized for 3D facial display," in *Proc. ACM SIGGRAPH Emerging Technol.*, vol. 28, 2013, Art. no. 3.

[7] A. Jones, I. Mcdowall, H. Yamada, M. Bolas, and P. Debevec, "Rendering for an interactive 360 light field display," *ACM Trans. Graph.*, vol. 26, no. 3, 2007, Art. no. 40.

[8] D. Lanman, M. Hirsch, Y. Kim, and R. Raskar, "Content-adaptive parallax barriers: Optimizing dual-layer 3D displays using low-rank light field factorization," *ACM Trans. Graph.*, vol. 29, no. 6, 2010, Art. no. 163.

[9] G. Wetzstein, D. Lanman, W. Heidrich, and R. Raskar, "Layered 3D: Tomographic image synthesis for attenuation-based light field and high dynamic range displays," *ACM Trans. Graph.*, vol. 30, no. 4, 2011, Art. no. 95.

[10] H. Takada, S. Suyama, K. Hiruma, and K. Nakazawa, "58.2: A Compact DepthFused 3D LCD," in *Proc. SID Symp. Dig. Tech. Papers*, 2003, pp. 1526–1529.

[11] D. Lanman, G. Wetzstein, M. Hirsch, W. Heidrich, and R. Raskar, "Polarization fields: Dynamic light field display using multi-layer lcds," *ACM Trans. Graph.*, vol. 30, no. 6, 2011, Art. no. 186.

[12] G. Wetzstein, D. R. Lanman, M. W. Hirsch, and R. Raskar, "Tensor displays: compressive light field synthesis using multilayer displays with directional backlighting," *ACM Trans. Graph.*, vol. 31, no. 4, pp. 1–11, 2012.

[13] M. Hirsch, G. Wetzstein, and R. Raskar, "A compressive light field projection system," *ACM Trans. Graph.*, vol. 33, no. 4, 2014, Art. no. 58.

[14] A. A. Lukianitsa and A. N. Putilin, "Stereodisplay with neural network image processing," in *Proc. SPIPE: Stereoscopic Displays Virtual Reality Syst. IX*, vol. 4660, 2002, pp. 207–211.

[15] H. Gotoda, "A multilayer liquid crystal display for autostereoscopic 3D viewing," *Proc. SPIE*, vol. 7524, no. Stereoscopic Displays and Applications XXI, pp. 75 240P 1–8, 2010.

[16] R. Chen, A. Maimone, H. Fuchs, R. Raskar, and G. Wetzstein, "Wide field of view compressive light field display using a multilayer architecture and tracked viewers," *J. Soc. Inf. Display*, vol. 22, no. 10, pp. 525–534, 2015.

[17] A. Maimone, G. Wetzstein, M. Hirsch, D. Lanman, R. Raskar, and H. Fuchs, "Focus 3D: Compressive Accommodation Display," *ACM Trans. Graph.*, vol. 32, no. 5, pp. 1–13, 2013.

[18] F.-C. Huang, K. Chen, and G. Wetzstein, "The light field stereoscope: Immersive computer graphics via factored near-eye light field displays with focus cues," *ACM Trans. Graph.*, vol. 34, no. 4, 2015, Art. no. 60.

[19] M. Date, T. Hisaki, H. Takada, S. Suyama, and K. Nakazawa, "Luminance addition of a stack of multidomain liquid-crystal displays and capability for depth-fused three-dimensional display application," *Appl. Opt.*, vol. 44, no. 44, pp. 898–905, 2005.

[20] H. Gotoda, "Design of time-multiplexed autostereoscopic displays based on virtual stacking of multi-layer panels," in *IS&T/SPIE Electron. Imag.*, 2013, pp. 2574–2576.

[21] O. Aharon, "Liquid crystal wavelength-independent continuous polarization rotator," *Opt. Eng.*, vol. 49, no. 3, 2010, Art. no. 034002.

[22] I. Moreno, J. L. Martínez, and J. A. Davis, "Two-dimensional polarization rotator using a twisted-nematic liquid-crystal display," *Appl. Opt.*, vol. 46, no. 6, 2007, Art. no. 881.

[23] G. Zhou, Q. Zhao, Y. Zhang, and A. Cichocki, "Fast nonnegative tensor factorization by using accelerated proximal gradient," in *Proc. Int. Symp. Neural Netw.*, 2014, pp. 459–468.

[24] F. Heide, D. Lanman, D. Reddy, J. Kautz, K. Pulli, and D. Luebke, "Cascaded displays: Spatiotemporal superresolution using offset pixel layers," *ACM Trans. Graph.*, vol. 33, no. 4, 2014, Art. no. 60.

[25] F. Heide, G. Wetzstein, R. Raskar, and W. Heidrich, "Adaptive image synthesis for compressive displays," *ACM Trans. Graph.*, vol. 32, no. 4, 2013, Art. no. 132.

[26] G. Andrew and J. Gao, "Scalable training of L1-regularized log-linear models," in *Proc. Int. Conf. Mach. Learn.*, vol. 24, 2007, pp. 33–40.

[27] C. Zhu, R. H. Byrd, P. Lu, and J. Nocedal, "Algorithm 778: L-BFGS-B: Fortran subroutines for large-scale bound-constrained optimization," *ACM Trans. Math. Softw.*, vol. 23, no. 4, pp. 550–560, 1997.

[28] S. S. Rao and S. S. Rao, *Engineering Optimization: Theory and Practice*. Hoboken, NJ, USA: John Wiley & Sons, 2009.

[29] R. Szeliski, *Computer Vision: Algorithms and Applications*. Berlin, Germany: Springer Science & Business Media, 2010.

[30] E. Adelson and C. Anderson, "Pyramid methods in image processing," *RCA Engineer*, vol. 29, no. 6, pp. 33–41, 1984.

[31] J.-Y. Bouguet, "Pyramidal implementation of the affine lucas kanade feature tracker-description of the algorithm," *Pages.Slc.Edu.*, vol. 2, 2001, Art. no. 3.

[32] X. Cao, Z. Geng, T. Li, M. Zhang, and Z. Zhang, "Accelerating decomposition of light field video for compressive multi-layer display," *Opt. Express*, vol. 23, no. 26, 2015, Art. no. 34007.

[33] M. Hirsch, D. Lanman, G. Wetzstein, and R. Raskar, "Construction and calibration of optically efficient LCD-based multi-layer light field displays," *J. Phys.: Conf. Series*, vol. 415, no. 1, 2013, Art. no. 12071.

[34] M. Schmidt, "minFunc: Unconstrained differentiable multivariate optimization in matlab," Software available at http://www.cs.ubc.ca/∼schmidtm/Software/minFunc.htm, 2005.

[35] M. W. Schmidt, E. V. D. Berg, M. P. Friedlander, and K. Murphy, "Optimizing costly functions with simple constraints: A limited-memory projected quasi-newton algorithm," in *Proc. Int. Conf. Artif. Intell. Statist.*, vol. 5, pp. 456–463, 2009.

[36] B. W Bader, T. G. Kolda, and Others, "MATLAB Tensor Toolbox Version 2.6," 2015.

[37] J. Wetzl, O. Taubmann, S. Haase, T. Köhler, M. Kraus, and J. Hornegger, "GPU-Accelerated Time-of-Flight Super-Resolution for Image-Guided Surgery," in *Bildverarbeitung Für Die Medizin*, 2013, pp. 21–26.

[38] M. Zwicker, W. Matusik, F. Durand, and H. Pfister, "Antialiasing for automultiscopic 3D displays," *Eurographics Symp. Rendering*, pp. 73–82, 2006.

Jiahui Zhang received his BS degree in Mechanical Engineering from Tsinghua University in 2015. He is now a PhD student in the Department of Biomedical Engineering, Tsinghua University, Beijing, China. His research interests include light field displays and 3D content generation via deep learning.

Zhencheng Fan received her BS degree in biomedical engineering from Tianjin University in 2013. She is now a PhD student in the Department of Biomedical Engineering, School of Medicine, Tsinghua University, Beijing, China. Her research interests include 3D display and application technologies, especially integral photography and surgical navigation.

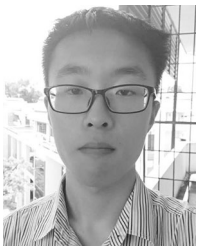

Dawei Sun is an undergraduate student in the Department of Automation, Tsinghua University, Beijing, China. His research interests include light field displays and self-driving cars.

Hongen Liao (M04, SM14) received his BS degree in mechanics and engineering sciences from Peking University, Beijing, China, in 1996 and his ME and PhD degrees in precision machinery engineering from the University of Tokyo, Tokyo, Japan, in 2000 and 2003, respectively. He was a Research Fellow of the Japan Society for the Promotion of Science. Since 2004, he has been a faculty member in the Graduate School of Engineering, University of Tokyo, where he became an Associate Professor in 2007. He has been selected as a National Thousand Talents Distinguished Professor by the National Recruitment Program of Global Experts, China, since 2010, and is currently a full Professor and the Vice Director in the Department of Biomedical Engineering, School of Medicine, Tsinghua University, Beijing, China. His research interests include 3D medical imaging, image-guided surgery, medical robotics, computer-assisted surgery, and the fusion of these techniques for minimally invasive precision diagnosis and therapy. He has also been involved in research on long-viewing-distance autostereoscopic displays and 3D visualization. He is the author and coauthor of more than 210 peer-reviewed articles and proceedings papers, as well as 32 patents, more than 290 abstracts and numerous invited lectures. He was distinguished by receiving a Commendation for Science and Technology from the Ministry of Education, Culture, Sports, Science and Technology (MEXT) of Japan. He has received more than ten awards, including the OGINO Award (2007), the Ericsson Young Scientist Award (2006), the IFMBE Young Investigators Awards (2005 and 2006), and various Best Paper Awards from different academic societies. His research has been well funded by MEXT, the Ministry of Internal Affairs and Communications, the New Energy and Industrial Technology Development Organization, the Japan Society for the Promotion of Science in Japan, and the National Natural Science Foundation of China. He is an Associate Editor of the IEEE Engineering in Medicine and Biology Society Conference and was the Organization Chair of the Medical Imaging and Augmented Reality Conference (MIAR) in 2008, the Program Chair of the Asian Conference on Computer-Aided Surgery (ACCAS) in 2008, 2009 and 2017, the Tutorial Co-chair of the Medical Image Computing and Computer Assisted Intervention Conference (MICCAI) in 2009, the Publicity Chair of MICCAI 2010, the General Chair of MIAR 2010 and ACCAS 2012, the Program Chair of MIAR 2013, the Workshop Chair of MICCAI 2013, and the General Co-chair of MIAR 2016. He is the President of the Asian Society for Computer Aided Surgery and the Secretary of the Asian-Pacific Activities Working Group of the International Federation for Medical and Biological Engineering (IFMBE).